

# A Model for Oxidative Pyrolysis of Corrugated Cardboard

MOLLIE R. SEMMES<sup>1</sup>, XUAN LIU<sup>1</sup>, MARK B. MCKINNON<sup>1</sup>, STANISLAV I. STOLIAROV<sup>1,\*</sup>, and ARTUR WITKOWSKI<sup>2</sup>

<sup>1</sup>Department of Fire Protection Engineering  
University of Maryland, College Park, MD, USA

<sup>2</sup>Centre for Fire Hazards Science  
University of Central Lancashire, Preston PR1 2HE, UK

## ABSTRACT

Pyrolysis of a double-wall corrugated cardboard was studied in anaerobic and oxygen containing atmospheres using thermogravimetric analysis and a newly developed Controlled Atmosphere Pyrolysis Apparatus (CAPA). Oxygen was shown to affect kinetics and thermodynamics of the cardboard degradation. A previously developed cardboard pyrolysis model, which was partially based on cone calorimetry tests, was demonstrated to reproduce anaerobic gasification experiments conducted in CAPA. This model was extended to include oxidation reactions and transport of oxygen inside the cardboard matrix. The extended model was validated against the mass loss rate data collected in CAPA at 10.5 vol.% of oxygen under incident radiant heat fluxes of 20, 40, and 60 kW m<sup>-2</sup>.

**KEYWORDS:** pyrolysis; thermal decomposition; smoldering; lignocellulosic materials

## INTRODUCTION

Warehouse storage can pose a potential fire hazard because of the orientation and nature of the storage containers and the stored commodities. Corrugated cardboard is frequently used to produce storage containers and, as a result, can serve as the primary fuel load in the initial stages of warehouse fires. The importance of the material to fires that begin in storage occupancies has led to several recent studies on corrugated cardboard to establish the flammability properties and behavior of the material [1-3], determine its effective thermal degradation mechanism [4], and investigate its role in fire growth for specific scenarios [5,6]. These studies have improved the understanding of warehouse fires and have contributed to the development of predictive Computational Fluid Dynamics (CFD) fire models that involve the combustion of corrugated cardboard.

Pyrolysis submodels for condensed-phase fuels defined in a CFD fire model generally describe in-depth heat transfer and thermal decomposition and are coupled to the gas-phase phenomena. These submodels solve energy and mass conservation equations to predict the gaseous fuel generation rate and solid surface temperature as a function of time and incident heat flux. Materials are defined in pyrolysis submodels by several thermo-physical properties. A systematic approach was presented in a related study in which data collected in thermogravimetric analysis (TGA), differential scanning calorimetry (DSC), and cone calorimetry tests accompanied by in-depth temperature measurements were analyzed to determine an effective reaction mechanism, define thermo-physical properties and develop a pyrolysis model for a double-wall corrugated cardboard [7].

The analysis of the cone calorimetry tests employed in the cardboard model development was complicated by the presence of a flame on the sample surface. While attempts were made to measure the flame heat flux to the sample, these measurements yielded somewhat uncertain results. The presence of the flame also led to the assumption that oxygen did not participate in the pyrolysis process. This assumption tended to lose validity toward the end of the cone calorimetry tests, where flame reduced in size to the point that it covered only a fraction of the material surface.

The purpose of the current study was to validate (and augment if necessary) the cardboard pyrolysis model that relied on the cone calorimetry tests and to extend this model to account for reaction of the cardboard with oxygen present at the material surface. To achieve this goal, a controlled-atmosphere pyrolysis apparatus (CAPA) was developed [8] as an addition to the standard cone calorimeter [9]. CAPA provided a capability to conduct radiant heating experiments on coupon-sized samples in a well-defined gaseous atmosphere.

\*Corresponding author. E-mail address: stolia@umd.edu.

The experiments conducted in CAPA in a gaseous atmosphere containing around 2 vol.% of oxygen (minimum achievable concentration) and balance of nitrogen were employed to validate previously developed (anaerobic) pyrolysis model. TGA tests conducted at 10 and 21 vol.% of oxygen in nitrogen and pyrolyzing material temperature measurements conducted in CAPA at 10.5 vol.% of oxygen (the highest concentration that prevented autoignition) were utilized to develop a quantitative description of cardboard oxidation kinetics and transport. The oxidative pyrolysis model was validated against mass loss rate data collected in CAPA at 10.5 vol.% of oxygen under incident radiant heat fluxes of 20, 40, and 60 kW m<sup>-2</sup>.

## EXPERIMENTAL

### Material

The samples used in this study were double-wall cardboard designated as 69-23B-69-23C-69. The numbers in the cardboard designation refer to the areal density of each layer in lb per 1000 ft<sup>2</sup>. The letters signify the flute designation. B-flute is characterized by  $160 \pm 10$  flutes per m and a layer height of  $2.1 \pm 0.2$  mm. C-flute is characterized by  $132 \pm 10$  flutes per m and a layer height of  $3.4 \pm 0.2$  mm. The thickness of the linerboards was measured as  $0.64 \pm 0.03$  mm. The measured density of the linerboards was  $520 \pm 50$  kg m<sup>-3</sup>. The composite density of the fluted layers was defined as the mass of the fluted medium over the volume of the entire layer. The composite density of the C-fluted section was measured as  $49 \pm 5$  kg m<sup>-3</sup> and the density of the B-fluted section was measured as  $74 \pm 7$  kg m<sup>-3</sup>. A schematic of the corrugated cardboard is provided in Figure 1

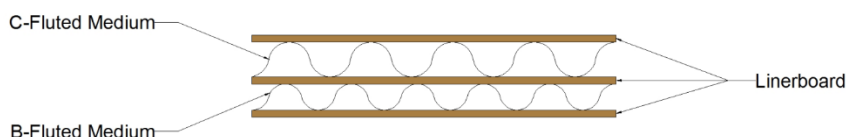


Figure 1. Schematic of Corrugated Cardboard Sample

### Thermogravimetric Analysis

Thermogravimetric analysis is a test method in which mass is measured as the temperature of the sample follows a heating program in a well-defined gas atmosphere. TGA tests were conducted with a Netzsch 449 F3 Jupiter simultaneous thermal analyzer. A file was used to grind the corrugated cardboard to form powder that was subsequently compacted to 6-10 mg, disc-like TGA samples. The tests were conducted in a moisture-free nitrogen atmosphere to collect data that was analyzed to determine the thermal degradation reaction mechanism for cardboard. The results of these tests and analyses are described in detail in a previous publication [7]. TGA tests conducted in the present study were performed in atmospheres of 10 and 21 vol.% of oxygen with balance of nitrogen to determine the impact of oxygen on the thermal degradation kinetics.

Cardboard powder was compacted in an alumina (Al<sub>2</sub>O<sub>3</sub>) crucible, which remained uncovered throughout each of the tests. The temperature program for all TGA tests consisted of heating from 313 K to 973 K at a rate of 10 K min<sup>-1</sup>. The sample mass and heating rate were selected to ensure that no significant concentration or temperature gradients existed within the sample. The gas flow rate was 50 mL min<sup>-1</sup> of N<sub>2</sub> (at the standard pressure and temperature) for the tests conducted in pure nitrogen, 54 mL min<sup>-1</sup> N<sub>2</sub> and 6 mL min<sup>-1</sup> O<sub>2</sub> for the 10% oxygen tests, and 49 mL min<sup>-1</sup> N<sub>2</sub> and 13 mL min<sup>-1</sup> O<sub>2</sub> for 21% oxygen tests.

### Controlled-Atmosphere Pyrolysis Experiments

Bench-scale tests for this study were conducted in a newly designed Controlled Atmosphere Pyrolysis Apparatus, which was added to a Govmark CC-1 cone calorimeter. A detailed schematic of this apparatus installed under the cone heater is shown in Figure 2. CAPA consists of two concentric square metal ducts connected at the bottom. Gas is introduced into the space between the ducts from the gas inlets in each of the four sides. The space above the gas inlets between the two ducts is filled with small (4.5 mm diameter) glass beads to ensure a uniform gas velocity. The upper edge of the inner duct is 10 mm below the top surface of the sample; the upper edge of the outer duct is 10 mm above the surface.

A material sample with dimensions of 80 by 80 mm is conditioned in a desiccator box for at least 48 hours before the test to ensure consistent water content. The sample is thermally insulated around the perimeter and mounted on top of 30 mm of Kaowool PM insulation. The sample and insulation are subsequently

secured on a stainless steel sample holder located at the center of the interior volume of the inner duct. The interior volume of the inner duct and sample holder each has a square cross section with sides measured 120 mm and 115 mm, respectively. The gap between these two is blocked by a lip installed on the sample holder (see Figure 2). The lip is located 1 mm above the upper edge of the inner duct, ensuring that the sample holder is suspended on the balance and does not make contact with the CAPA ducts to prevent mass measurement interference.

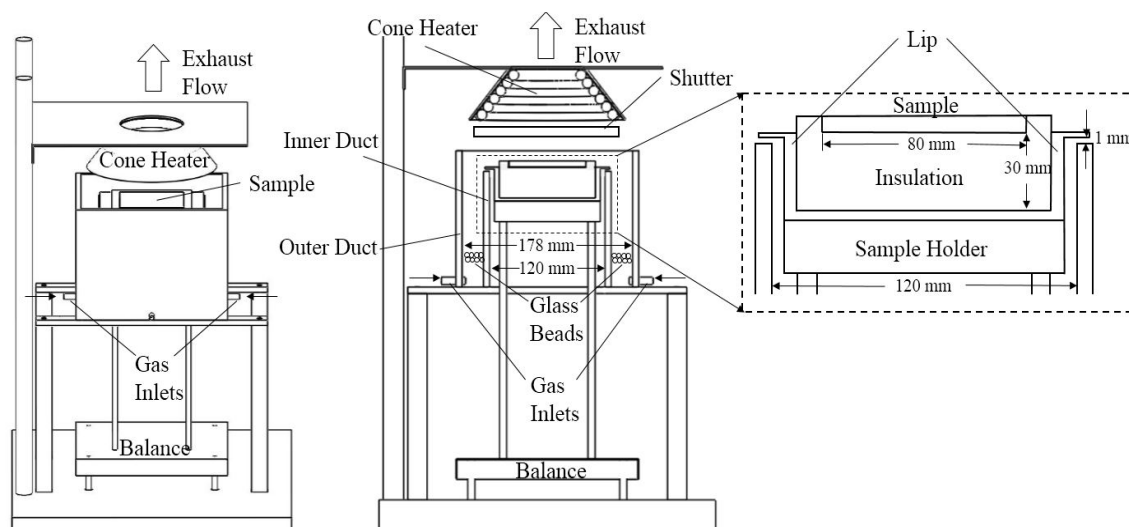


Figure 2. Schematic of Controlled Atmosphere Pyrolysis Apparatus

A Schmidt-Boelter heat flux gauge was positioned at a location corresponding to the geometric center of the top sample surface, 40 mm below the bottom of the cone heater, to set the radiant heat flux to the sample. A feedback control system of the cone calorimeter automatically adjusted the temperature of the heater based on the signal from the heat flux gauge. The uniformity of the heat flux at the sample surface was examined with a separate heat flux gauge and found to be satisfactory ( $< 5\%$  maximum deviation from the set point).

The gas flow rates to CAPA were set using ALICAT MCR series mass flow controllers. The total gas flow was maintained at  $225 \text{ L min}^{-1}$  (at the standard pressure and temperature) in all experiments. The gas temperature was measured at the level of the top sample surface in the middle between the ducts using a thin (0.13 mm diameter) type K thermocouple. The temperature was found to be somewhat dependent on the radiant heat flux changing linearly from 330 to 370 K as the heat flux increased from 20 to  $60 \text{ kW m}^{-2}$ . The mean in-duct gas velocity, which was computed from the mass flow and temperature data, was found to be around  $0.3 \text{ m s}^{-1}$  (essentially independent of heating conditions). The cone calorimeter exhaust system was set to operate at the standard flow rate of  $1440 \text{ L min}^{-1}$  [9]. The experimental system was open to the atmosphere.

Feeding  $225 \text{ L min}^{-1}$  of  $\text{N}_2$  to CAPA resulted in  $2.2 \pm 0.4 \text{ vol.}\%$  concentration of  $\text{O}_2$  at the surface of the sample. This condition was assumed to be essentially anaerobic (taking into account a moderate sensitivity of the cardboard material to oxygen demonstrated in TGA experiments). Feeding  $135 \text{ L min}^{-1}$  of  $\text{N}_2$  and  $90 \text{ L min}^{-1}$  of air produced  $10.5 \pm 0.4 \text{ vol.}\%$  of  $\text{O}_2$  at the surface, which represented near-critical oxygen concentration for auto-ignition of the cardboard at a heat flux of  $60 \text{ kW m}^{-2}$  (a reproducible autoignition was observed at around 14 vol.% of  $\text{O}_2$ ). The oxygen concentration was measured by continuously sampling from the atmosphere at a range of horizontal locations 1 mm above the top sample surface and analyzing this atmosphere with Servomex 4100 gas analyzer.

No flame was present at the sample surface in any of the pyrolysis experiments. To quantify convective heat losses from the top surface, a 3 mm thick copper plate of sample dimensions was placed into CAPA instead of a sample. The plate was painted black for a well-defined emissivity of 0.95 and was equipped with several imbedded type K thermocouples. The measurements of the plate temperature were performed at 20, 40 and  $60 \text{ kW m}^{-2}$  of incident radiant heat flux. Modeling of these experiments was utilized to determine the convection coefficient, which was the only unknown parameter. Setting this parameter to 5

$\text{W m}^{-2} \text{K}^{-1}$  was found to produce the best agreement between the experimental and simulated copper temperatures. Details of this convection coefficient determination procedure are provided elsewhere [8].

The tests conducted on the corrugated cardboard were performed at the above referenced oxygen concentrations and radiant heat fluxes of 20, 40 and 60  $\text{kW m}^{-2}$ . The mass and temperatures of the sample were measured as a function of time in separate tests. The temperatures were obtained using 0.25 mm diameter shielded type K thermocouples inserted in the top and bottom linerboard sections at a central point such that the bead of the thermocouple was located at the approximate middle of the cardboard specimen and the thermocouple wire was perpendicular to the main direction of heat flow. Three to five tests were conducted at each flux, oxygen concentration and for each type of measurement.

## MODELING

The ThermaKin modeling environment [10] was employed to extract properties from experimental data and to construct a one-dimensional pyrolysis model to predict the results of bench scale tests. ThermaKin solves non-steady energy and mass conservation equations for chemical reactions described by finite-rate chemical kinetics. Each material component defined in the model is characterized by a set of thermo-physical properties that describe heat transfer and mass transport in the condensed phase. Reactions are governed by the Arrhenius law and can be specified to be of the first or second order.

Mass transport and heat transfer boundary conditions for convective and radiative heat flow are defined at the top and bottom surfaces of the computational domain to represent the conditions of the simulated experiment. The environmental temperature can be defined as a linear function of time to modify the convective heat flow boundary condition during simulation. The radiative heat flow boundary condition can be specified with a maximum of three heat flux phases that may vary linearly with respect to time and may be specified as periodic. Details concerning the conservation equations, treatment of boundary conditions, and all other functionality in the ThermaKin program are provided elsewhere [10].

## EXPERIMENTAL RESULTS AND MODEL DEVELOPMENT

### Existing Model Summary

This section presents a summary of the model developed in a previous study [7]. The experimental methods and subsequent analysis conducted to parameterize the model are briefly described. This model was shown to predict times to ignition and mean mass loss rates measured in cone calorimetry tests (flaming combustion) at 20-80  $\text{kW m}^{-2}$  of external heat flux to within, on average, 2 s and 17%, respectively.

Analysis of the TGA data collected in nitrogen led to an effective reaction mechanism with one reaction describing the release of residual moisture and three consecutive reactions describing the thermal decomposition of cardboard. The reaction parameters, which include the pre-exponential factor ( $A$ ), activation energy ( $E$ ), and the stoichiometric coefficients ( $\nu$ ), are provided in Table 1. Reaction 1 corresponds to the liberation of residual moisture ( $\text{H}_2\text{O}_\ell \rightarrow \text{H}_2\text{O}_g$ ); reactions 2-4 represent thermal decomposition. Reaction 2 represents the initial, dried cardboard decomposition to a solid intermediate (referred to by the subscript *int*) and gas. Reaction 3 represents the decomposition of the intermediate species to an initial char (*char1*) and gas. Reaction 4 corresponds to decomposition of the initial char to the final residual char (*char2*) and gas. The heat capacities ( $c$ ) of all components representing cardboard and the heats of the decomposition reactions ( $h_r$ ) were determined through the analysis of data collected in DSC tests. The endothermic heat of the overall decomposition was assigned to the reaction in which the largest mass was volatilized (reaction 3 in Table 1); the heat of vaporization for water was assigned to the moisture liberation reaction.

Table 1. Reaction Parameters for Corrugated Cardboard Thermal Degradation

Reaction	$A \text{ (s}^{-1}\text{)}$	$E \text{ (J mol}^{-1}\text{)}$	$\nu^{\text{solid}}$	$\nu^{\text{gas}}$	$h_r \text{ (J g}^{-1}\text{)}$
1	6.1	$2.35 \times 10^4$	0	1	$-2.4 \times 10^3$
2	$8.0 \times 10^9$	$1.30 \times 10^5$	0.90	0.10	0
3	$2.0 \times 10^{11}$	$1.60 \times 10^5$	0.37	0.63	$-1.3 \times 10^2$
4	$2.6 \times 10^{-2}$	$1.70 \times 10^4$	0.59	0.41	0

The cardboard sample (see Figure 1) was represented in the model with separate components defined for the linerboard (*LB*), C-fluted layer (*CFL*), B-fluted layer (*BFL*), and residual moisture ( $H_2O_g$ ). Each solid layer was assigned a thickness and density equal to the corresponding mean measured value.  $H_2O_g$  was distributed uniformly among layers at 2 mass% concentration. Each of the components present after the release of residual moisture (*LB*, *CFL*, and *BFL*) had a unique density ( $\rho$ ), and was found to decompose according to the three-reaction sequence identified in Table 1 (reactions 2-4). The density of each solid decomposition product was defined as the reactant component density multiplied by the stoichiometric coefficient of the solid product for the corresponding reaction. Defining densities in this manner expanded the decomposition mechanism from three reactions to nine and ensured the thickness of the sample did not change during degradation, which agreed with experimental observations.

The thermal conductivity ( $\kappa$ ) and emissivity ( $\epsilon$ ) of the initial components were determined through an inverse analysis of in-depth temperature profiles collected prior to ignition in which the objective variable was adjusted to improve the agreement between the predicted and experimental profiles. The thermal conductivity was determined based on data collected with the surface of the samples painted for an emissivity of 0.95. The emissivity of the initial components was determined based on temperature profile data collected from unaltered samples.

The thermal transport properties of the char components were determined through an inverse analysis in a procedure similar to the one used to determine the thermal transport properties of the initial components. The observed structure and the high temperature of the char components led to the hypothesis that radiative heat transfer dominated when the char was formed. The radiation-diffusion approximation [11] was invoked to describe the radiative heat transfer through heat conduction mathematics by defining an effective temperature-dependent thermal conductivity for the char components. The effective thermal conductivity was assumed to be inversely proportional to the density of the char, which led to an effective thermal conductivity of the decomposed fluted layers an order of magnitude larger than that of the decomposed linerboard.

The emissivity of the char components was assumed to be equivalent to the emissivity of graphite at the temperature range in which the char was produced [12]. The thermal properties of each intermediate component were defined as the mean of the property of the initial and final solid component in the same reaction path. These assumed relationships reduced the representation of the thermal transport properties for all components representing solid degradation products to a single independent variable that was determined through an inverse analysis. The mean instantaneous deviation between the final model temperature profiles determined through the inverse analysis and the experimental temperature profiles was less than 5% for the 20 kW m<sup>-2</sup> case. A complete summary of the physical parameters used to construct the model including the properties of sample backing material, Kaowool PM, and component representing all gaseous decomposition products ( $CB_{vol}$ ) is provided in Table 2.

Table 2. Thermo-physical Properties of Corrugated Cardboard Components and Backing Material

Component	$\rho$ (kg m <sup>-3</sup> )	$c$ (J g <sup>-1</sup> K <sup>-1</sup> )	$\kappa$ (W m <sup>-1</sup> K <sup>-1</sup> )	$\epsilon$
$H_2O_g$	--	$5.2 - 6.7 \times 10^{-3}T + 1.1 \times 10^{-5}T^2$	--	--
$H_2O_g$	--	$2.4 - 1.6 \times 10^{-3}T + 2.0 \times 10^{-6}T^2$	--	--
<i>LB</i>	520	1.8	0.10	0.70
<i>LB<sub>int</sub></i>	470	1.55	$0.05 + 7.5 \times 10^{-11}T^3$	0.78
<i>LB<sub>char1</sub></i>	170	1.3	$1.5 \times 10^{-10}T^3$	0.85
<i>LB<sub>char2</sub></i>	100	1.3	$1.5 \times 10^{-10}T^3$	0.85
<i>CFL</i>	49	1.8	0.10	0.70
<i>CFL<sub>int</sub></i>	44	1.55	$0.05 + 7.5 \times 10^{-10}T^3$	0.78
<i>CFL<sub>char1</sub></i>	16	1.3	$1.5 \times 10^{-9}T^3$	0.85
<i>CFL<sub>char2</sub></i>	9.4	1.3	$1.5 \times 10^{-9}T^3$	0.85
<i>BFL</i>	74	1.8	0.10	0.70
<i>BFL<sub>int</sub></i>	67	1.55	$0.05 + 7.5 \times 10^{-10}T^3$	0.78
<i>BFL<sub>char1</sub></i>	25	1.3	$1.5 \times 10^{-9}T^3$	0.85
<i>BFL<sub>char2</sub></i>	15	1.3	$1.5 \times 10^{-9}T^3$	0.85
$CB_{vol}$	--	1.3	--	--
Kaowool PM	256	1.07	$0.052 - 4 \times 10^{-5}T + 1 \times 10^{-7}T^2$	--

## Anaerobic Pyrolysis

The temperatures in the middle of the top and bottom linerboards measured in anaerobic CAPA experiments conducted at 20, 40 and 60 kW m<sup>-2</sup> of radiant heat flux are shown in Figure 3 as points. These points represent averaged data from 3-5 individual tests. The uncertainties (shown as error bars) are calculated from scatter of the experimental data as two standard deviations of the mean.

Figure 3 also shows calculated temperatures that were obtained with ThermaKin using the parameter set described in the previous section and boundary conditions corresponding to those measured in the CAPA experiments. The average instantaneous deviation between the model and the experimental data increases from 3 to 5% with increasing heat flux. These deviations are similar in magnitude to those observed in modeling of the cone calorimetry experiments based on which this parameter set was developed.

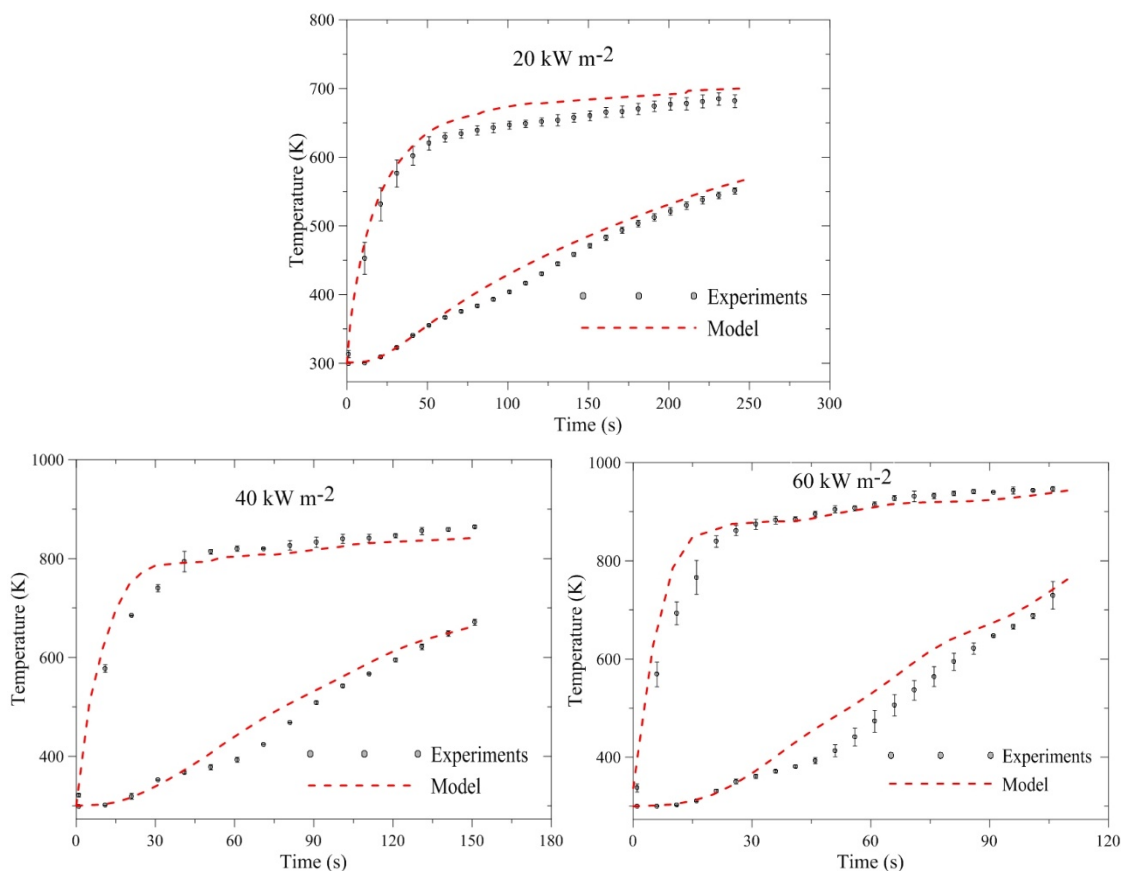


Figure 3. Comparison of Experimental and Simulated Temperature Histories of the Top and Bottom Linerboards Obtained for Anaerobic Pyrolysis

Experimental and simulated mass loss rate histories obtained under the same conditions as the aforementioned temperature profiles are provided in Figure 4. The height and timing of the modeled first mass loss rate peak agree well with the experiments. The subsequent modeled mass loss rate profile shows more emphasized fluctuations (associated with a sequential decomposition of the linerboards) than the experimental data. The average mass loss rate is underpredicted by the model by 10, 16 and 14% at 20, 40 and 60 kW m<sup>-2</sup>, respectively.

As in the case of temperature, the discrepancies between the simulated and experimental mass loss rate profiles are similar in structure and magnitude to those observed in modeling of the cone calorimetry experiments. These discrepancies are likely caused by slight reductions in the horizontal dimensions of pyrolyzing samples, which result in partial exposure of the sample side surfaces to radiant heat flux and flame (in the case of cone calorimetry). The other possible source of discrepancies is associated with uncertainties in the amount of moisture in the samples. While the samples were dried thoroughly, immediately prior to experiments, they were exposed to laboratory atmosphere the humidity of which was

not controlled. Overall, the current results indicate that the approximations of the flame heat flux behavior and anaerobic nature of cardboard degradation made during the analysis of previously conducted cone calorimetry tests [7] are reasonably accurate.

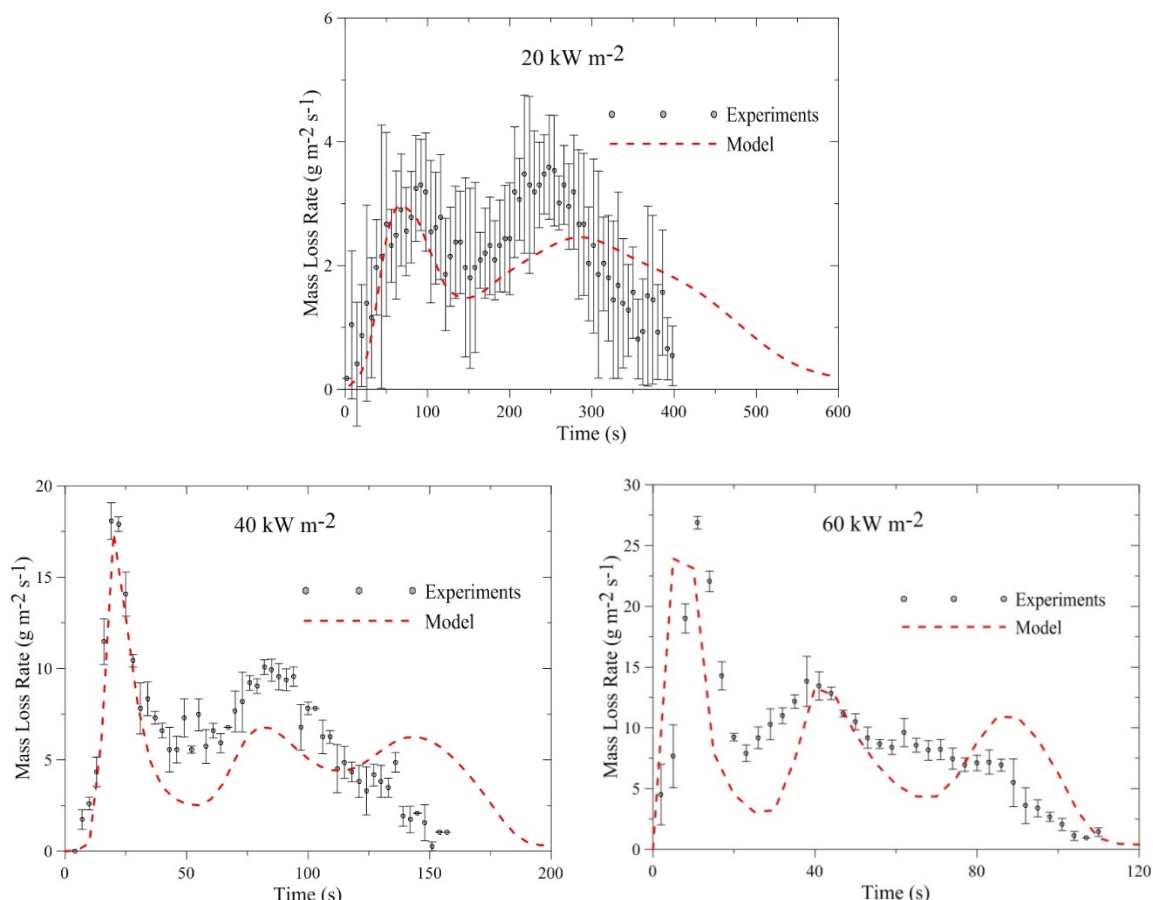


Figure 4. Comparison of Experimental and Simulated Mass Loss Rate Histories obtained for Anaerobic Pyrolysis

### Kinetics of Oxidation

The reaction mechanism defined in the previously constructed pyrolysis model was developed based on data collected in TGA tests conducted in a nitrogen atmosphere. In this study, additional TGA tests were performed in atmospheres with 10 and 21 vol.% of  $\text{O}_2$  in  $\text{N}_2$  to extend the definition of the reaction mechanism to oxygen-containing environments. The normalized mass and normalized mass loss rate curves collected in these TGA tests together with the results of anaerobic TGA experiments (shown here for comparison) are provided in Figure 5. The solid lines represent averages of three tests, which showed little scatter. This figure also contains modeled TGA data (dashed lines) that are explained below.

Introducing oxygen to the TGA tests caused the formation of a second major peak in the mass loss rate curve. Increasing the oxygen concentration tended to increase the maximum mass loss rate at both peaks and decrease the temperature range over which solid was volatilized. The final residue yield for the TGA tests decreased from 18.5% in nitrogen to approximately 5% in oxygenated atmospheres.

The analysis of the TGA data was performed using ThermaKin, which was run in a thermally thin mode. During this analysis, it was assumed that the oxygen concentration inside the solid samples was constant and equal to its concentration in the purge gas at the average material degradation temperature ( $\approx 625 \text{ K}$ ) and atmospheric pressure (101 kPa). The rates of oxygen-induced reactions were assumed to obey second order kinetics; i.e., these rates were set to be proportional to the solid reactant and oxygen concentrations (expressed in  $\text{g m}^{-3}$ ).

Four additional reactions were added to the anaerobic reaction mechanism (summarized in Table 1) to describe changes in the mass loss rate curves induced by oxygen. Addition of new reactions, rather than modification of the existing mechanism, ensured that the kinetic model reverts to the anaerobic thermal decomposition mechanism in the absence of oxygen. The parameters of the additional reactions were varied to achieve the best fit of the experimental TGA curves using an approach described in detail elsewhere [13]. The results of this fitting procedure are shown in Figure 5.

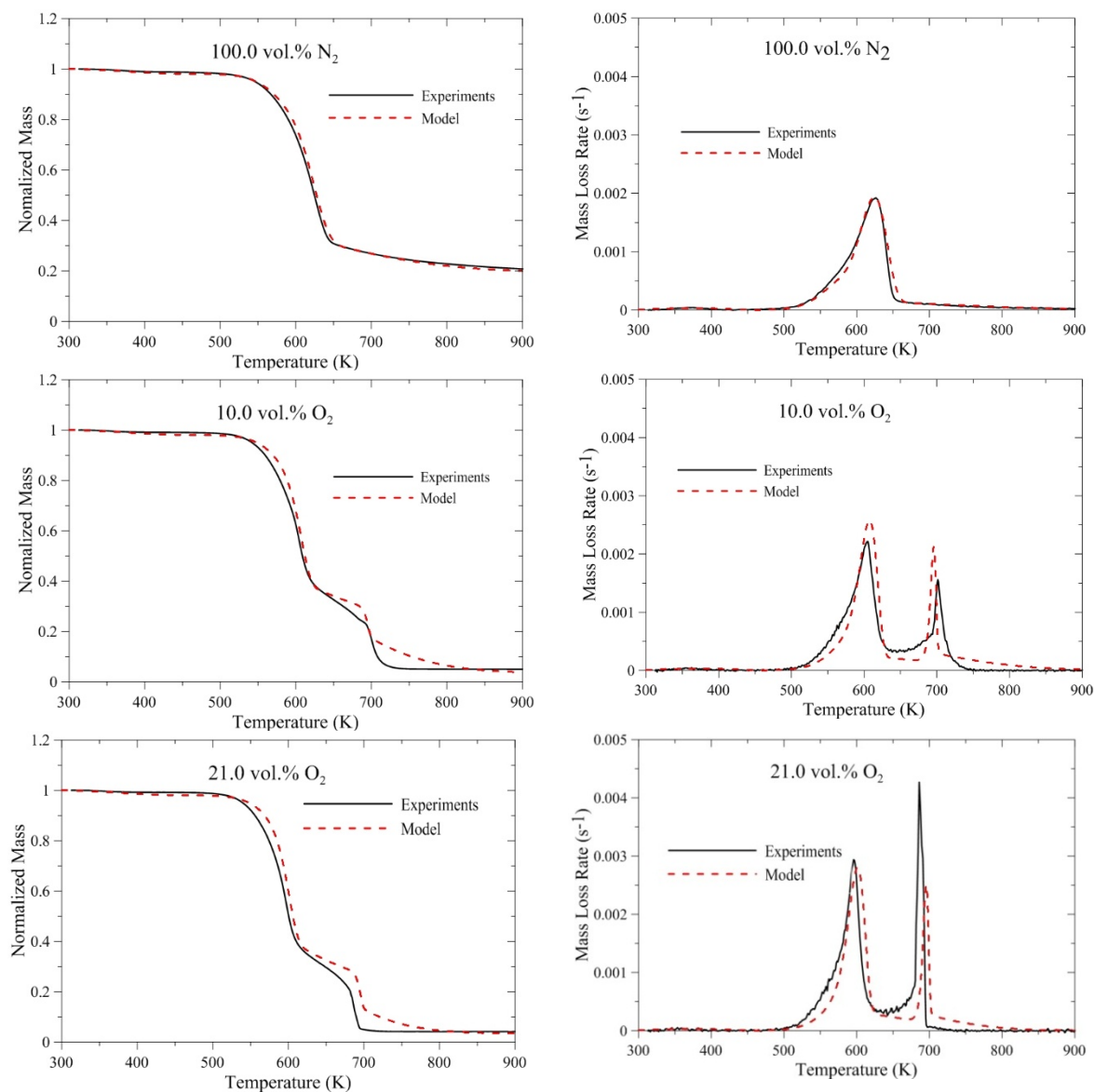


Figure 5. Experimental and Simulated TGA Curves Obtained at a Heating Rate of  $10 \text{ K min}^{-1}$

The final reaction mechanism, which represents both anaerobic and oxidative degradation, is provided in Table 3. The decomposition reactions are shown only for the linerboard component (*LB*) to avoid repetition of the same parameters for the components representing fluted layers (*CFL* and *BFL*). Two oxygen-induced reactions, reactions 3a and 3b, were added in parallel with the second anaerobic decomposition reaction, reaction 3 (which was present in the original model). One more oxygen-induced reaction, reaction 4a, was added in parallel to the third anaerobic decomposition reaction, reaction 4 (which was also present in the original model). The properties of the products of these oxygen-induced reactions were assumed to be the same as those of the products of the parallel anaerobic reactions. A final reaction, reaction 5, was included to describe oxidation of the fully decomposed char (*char2*) to final residue (*ash*).



The stoichiometric coefficients in front of the solid degradation products were determined from the TGA data. The heats of oxygen-induced reactions and stoichiometric coefficients in front of the oxygen were determined from the temperature measurements described in the next section.

Table 3. Oxidative and Non-Oxidative Degradation Reactions of Corrugated Cardboard

#	Reaction	$A$	$E$ (J mol <sup>-1</sup> )	$h_r$ (J g <sup>-1</sup> )
1	$1\text{H}_2\text{O}_\ell \rightarrow 1\text{H}_2\text{O}_g$	$6.1 \text{ s}^{-1}$	$2.35 \times 10^4$	$-2.4 \times 10^3$
2	$1\text{LB} \rightarrow 0.9\text{LB}_{\text{int}} + 0.1\text{CB}_{\text{vol}}$	$8.0 \times 10^9 \text{ s}^{-1}$	$1.30 \times 10^5$	0
3	$1\text{LB}_{\text{int}} \rightarrow 0.37\text{LB}_{\text{char1}} + 0.63\text{CB}_{\text{vol}}$	$2.0 \times 10^{11} \text{ s}^{-1}$	$1.60 \times 10^5$	$-1.3 \times 10^2$
3a	$1\text{LB}_{\text{int}} + 0\text{O}_2 \rightarrow 0.59\text{LB}_{\text{char1}} + 0.41\text{CB}_{\text{vol}}$	$7.5 \times 10^{11} \text{ m}^3 \text{ kg}^{-1} \text{ s}^{-1}$	$1.60 \times 10^5$	0
3b	$1\text{LB}_{\text{int}} + 0\text{O}_2 \rightarrow 0.48\text{LB}_{\text{char1}} + 0.52\text{CB}_{\text{vol}}$	$1.7 \times 10^{23} \text{ m}^3 \text{ kg}^{-1} \text{ s}^{-1}$	$2.80 \times 10^5$	0
4	$1\text{LB}_{\text{char1}} \rightarrow 0.59\text{LB}_{\text{char1}} + 0.41\text{CB}_{\text{vol}}$	$2.6 \times 10^{-2} \text{ s}^{-1}$	$1.70 \times 10^4$	0
4a	$1\text{LB}_{\text{char1}} + 0.95\text{O}_2 \rightarrow 0.48\text{LB}_{\text{char1}} + 1.47\text{CB}_{\text{vol}}$	$0.18 \text{ m}^3 \text{ kg}^{-1} \text{ s}^{-1}$	$1.70 \times 10^4$	$1.25 \times 10^4$
5	$1\text{LB}_{\text{char2}} + 1.56\text{O}_2 \rightarrow 0.15\text{LB}_{\text{ash}} + 2.4\text{CB}_{\text{vol}}$	$1.2 \times 10^{80} \text{ m}^3 \text{ kg}^{-1} \text{ s}^{-1}$	$1.08 \times 10^6$	$2.04 \times 10^4$

### Pyrolysis in the Presence of Oxygen

The temperatures in the middle of the top and bottom linerboards measured at 10.5 vol.% of oxygen in CAPA experiments are shown in Figure 6 along with the temperatures from the corresponding anaerobic (2.2 vol.% of O<sub>2</sub>) experiments. The data indicate that the presence of oxygen produces a significant increase in the material temperatures. This increase is most pronounced at low radiant heat fluxes.

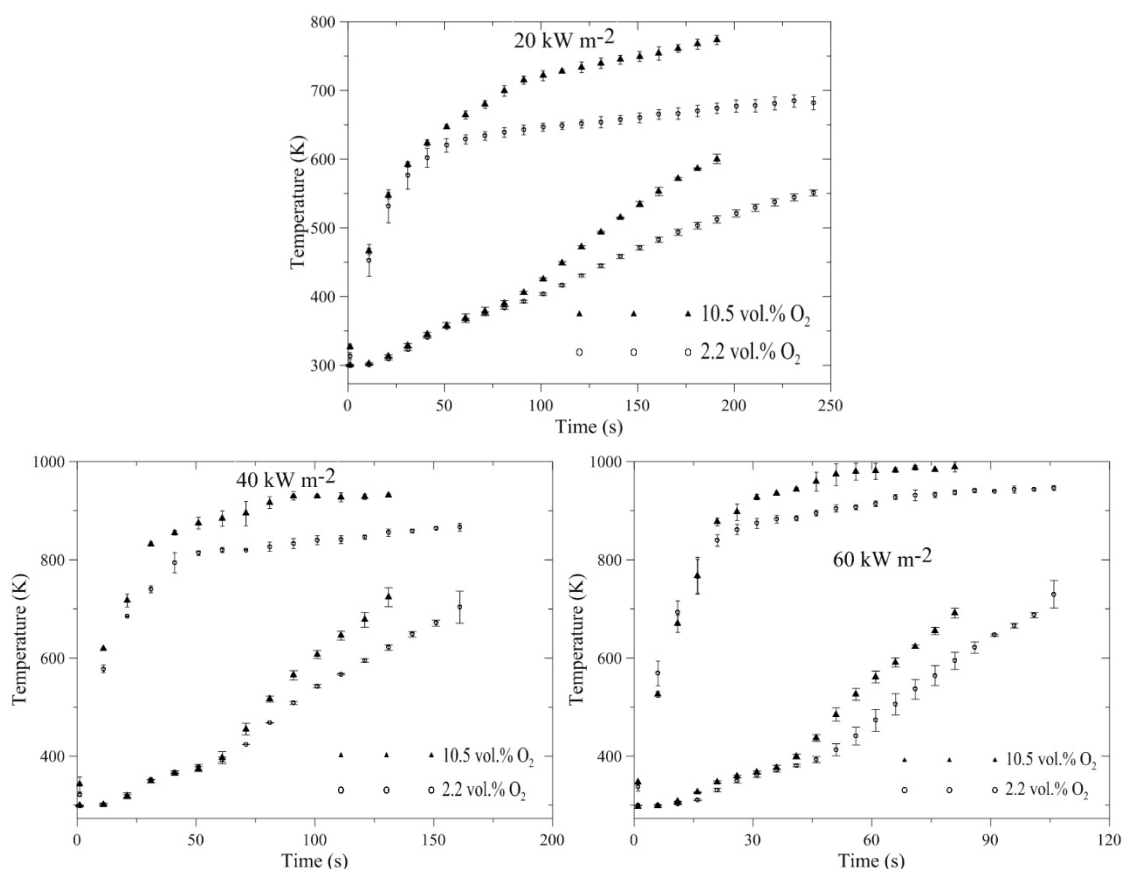


Figure 6. Comparison of Experimental Temperature Histories of the Top and Bottom Linerboards Obtained in Oxidative and Anaerobic Gaseous Atmospheres

The oxidative pyrolysis temperature data were employed to determine the heats of oxygen-induced reactions and the gas transfer coefficient, which defined the rate of mass transport of oxygen and all

gaseous decomposition products inside the solid. A detailed description of the mathematics of mass transport implemented in ThermaKin is provided elsewhere [10]. The heat capacity of oxygen was taken from NIST-JANAF tables [14]. The densities of *ash* components ( $LB_{ash}$ ,  $CFL_{ash}$  and  $BFL_{ash}$ ) were computed in the same manner as other solid decomposition product densities (see Existing Model Summary Section). The heat capacities, emissivities and thermal conductivities of *ash* components were assumed to be the same as those of the corresponding *char2* components. A summary of these property values is provided in Table 4.

Table 4. Thermo-physical Properties of Components Involved in Oxidative Degradation

Component	$\rho$ (kg m <sup>-3</sup> )	$c$ (J g <sup>-1</sup> K <sup>-1</sup> )	$\kappa$ (W m <sup>-1</sup> K <sup>-1</sup> )	$\epsilon$
O <sub>2</sub>	--	$0.83 + 3.5 \times 10^{-4} T - 8.9 \times 10^{-8} T^2$	--	--
$LB_{ash}$	15	1.3	$1.5 \times 10^{-10} T^3$	0.85
$CFL_{ash}$	1.4	1.3	$1.5 \times 10^{-9} T^3$	0.85
$BFL_{ash}$	2.3	1.3	$1.5 \times 10^{-9} T^3$	0.85

Initial simulations indicated that an assignment of exothermic heat values to reactions 4a and 5 (see Table 3) produces significantly better agreement between the model and experiments than adding heat to reactions 3a and 3b. Therefore, reactions 3a and 3b were set to be thermally neutral. The ratio of heats of reaction 4a and 5 was assumed to be equal the ratio of the fractions of the solid reactant volatilized in each process. The stoichiometric coefficients of the oxygen were assumed to be related to the heat of reaction through the Huggett rule, which states that 13.1 kJ of heat is released per 1 g of consumed O<sub>2</sub> [15]. These relationships reduced the number of unknown parameters to two, the total heat of reactions 4a and 5 and the gas transfer coefficient. These parameters were adjusted to fit the oxidative pyrolysis temperatures. The results of this fitting exercise, obtained with the heats of reaction reported in Table 3 and the gas transfer coefficient equal to  $1 \times 10^{-5}$  m<sup>2</sup> s<sup>-1</sup>, are shown in Figure 7.

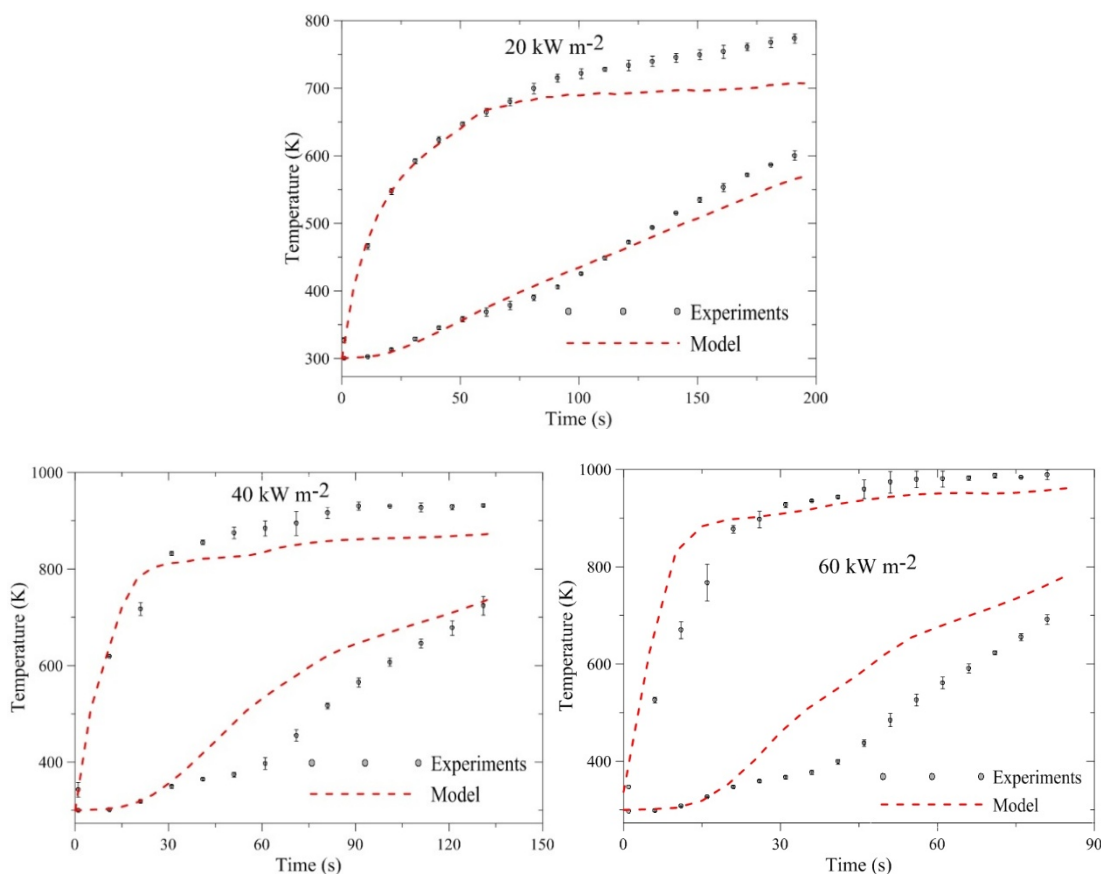


Figure 7. Comparison of Experimental and Simulated Temperature Histories of the Top and Bottom Linerboards Obtained for Pyrolysis in the Presence of 10.5 vol.% of Oxygen

The average instantaneous deviation between the modeled and experimental temperature data increases from 4 to 11% with increasing radiant heat flux. These deviations are notably larger than those observed for anaerobic pyrolysis. A comparison of the mass loss rates calculated using the fully parameterized model with the results of the mass loss rate measurements performed under the same conditions as aforementioned temperature measurements is shown in Figure 8. It is important to note that the experimental mass loss rate profiles were not used in the model parameterization. Therefore, this comparison should serve as an objective indicator of the validity of the model.

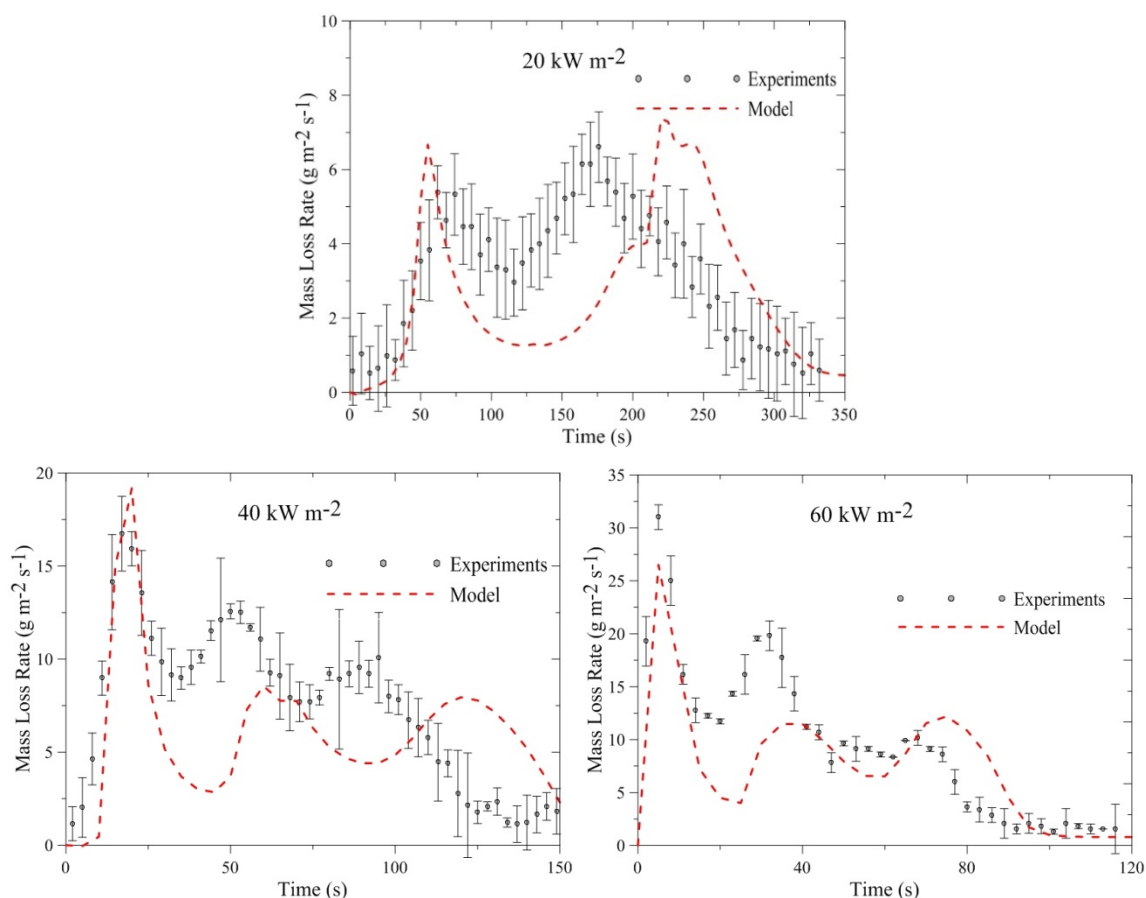


Figure 8. Comparison of Experimental and Simulated Mass Loss Rate Histories obtained for Pyrolysis in the Presence of 10.5 vol.% of Oxygen

The height and timing of the first mass loss rate peak are predicted well. The average mass loss rate is underpredicted by 15, 20 and 19% at 20, 40 and 60 kW m<sup>-2</sup>, respectively. As in the case of anaerobic pyrolysis, these deviations are thought to be associated primarily with a breakdown of the one-dimensional geometry of the experimental setup (due to shrinkage of degrading samples) and sample moisture unaccounted for in the model. The choice of the gas transfer coefficient did not have apparent impact on the rate of removal of volatile products from the degrading solid; i.e., when the fitted gas transfer coefficient ( $1 \times 10^{-5} \text{ m}^2 \text{ s}^{-1}$ ) was employed to simulate the anaerobic pyrolysis experiments, which were initially simulated using a default value of the gas transfer coefficient,  $2 \times 10^{-5} \text{ m}^2 \text{ s}^{-1}$ , the results showed no significant changes in the mass loss rate or temperature profiles.

## CONCLUSIONS

Controlled atmosphere pyrolysis experiments were performed on a double-wall corrugated cardboard in essentially anaerobic and oxygen-containing environments. A new apparatus (Controlled Atmosphere Pyrolysis Apparatus or CAPA) was developed to make it possible to conduct these experiments using the balance, radiant heater and exhaust system of a standard cone calorimeter. The material temperature histories measured in CAPA together with the results of TGA tests performed at several oxygen

concentrations were utilized to extend a previously developed anaerobic pyrolysis model of the cardboard material to oxidative conditions. The extended model was shown to predict the mass loss rate histories measured in CAPA at a wide range of radiant heat fluxes and in both oxidative and anaerobic gaseous environments with a reasonable degree of accuracy.

One process that was not included in the model, which might be important for a large scale cardboard fire, is a mechanical removal of partially degraded material by buoyancy-induced gas flow adjacent to the material's surface. This process may be a subject of future investigation. The processes observed in the current study were similar to those operating in smoldering combustion. However, this term was not used to describe these processes because the overall phenomenon did not conform to a formal definition of smoldering. According to the SFPE Handbook [16], smoldering combustion is a slow, low-temperature, flameless form of combustion, sustained by the heat evolved when oxygen directly attacks the surface of a condensed-phase fuel. Even in the presence of oxygen, the mass loss observed in the current experiments was dominated by the thermal decomposition rather than solid oxidation reactions. The heat produced in these reactions was not sufficient to sustain the mass loss.

## ACKNOWLEDGEMENTS

The authors would like to thank FM Global and NIST-ARRA program for providing funding for this research. Jing Li and Olga Zeller of The University of Maryland assisted with the design and conducting of experiments. Dr. Takashi Kashiwagi and Mr. Kenneth Steckler of NIST aided in the development of the CAPA. The authors are also grateful to Dr. Marcos Chaos and Dr. Sergey Dorofeev of FM Global for providing the corrugated cardboard samples and for valuable correspondence.

## REFERENCES

- [1] Gollner, M.J., Overholt, K., Williams, F.A., Rangwala, A.S., and Perricone, J., (2011) Warehouse Commodity Classification from Fundamental Principles. Part I: Commodity & Burning Rates, Fire Safety Journal 46: 305-316, <http://dx.doi.org/10.1016/j.firesaf.2011.03.002>
- [2] Overholt, K.J., Gollner, M.J., Perricone, J., Rangwala, A.S., and Williams, F.A., (2011) Warehouse Commodity Classification from Fundamental Principles. Part II: Flame Heights and Flame Spread, Fire Safety Journal 46: 317-329, <http://dx.doi.org/10.1016/j.firesaf.2011.05.002>
- [3] Chaos, M., Khan, M.M., Krishnamoorthy, N., Chatterjee, P., Wang, Y., and Dorofeev, S.B., Experiments and Modeling of Single- and Triple-wall Corrugated Cardboard: Effective Material Properties and Fire Behavior, Fire and Materials 2011, pp. 625-636.
- [4] David, C., Salvador, S., Dirion, J.L., and Quintard, M., (2003) Determination of a Reaction Scheme for Cardboard Thermal Degradation using Thermal Gravimetric Analysis, Journal of Analytical and Applied Pyrolysis 67: 307-323, [http://dx.doi.org/10.1016/S0165-2370\(02\)00070-0](http://dx.doi.org/10.1016/S0165-2370(02)00070-0)
- [5] Chaos, M., Wang, Y., Dorofeev, S.B., CFD Modeling of Flame Spread over Corrugated Cardboard Panels, International Congress on Fire Computer Modeling, 2012.
- [6] Chaos, M., Khan, M.M., Dorofeev, S.B., (2013) Pyrolysis of Corrugated Cardboard in Inert and Oxidative Environments, Proceedings of the Combustion Institute 34: 2583-2590, <http://dx.doi.org/10.1016/j.proci.2012.06.031>
- [7] McKinnon, M.B., Stoliarov, S.I., and Witkowski, A., (2013) Development of a Pyrolysis Model for Corrugated Cardboard, Combustion and Flame 160: 2595-2607, <http://dx.doi.org/10.1016/j.combustflame.2013.06.001>
- [8] Liu, X., (2012) Design and Analysis of New Gasification Apparatus based on the Standard Cone Calorimeter (Master's thesis). Retrieved from Proquest Dissertations and Theses. Publication No. 1529340.
- [9] ASTM Standard E1354 - 13, Standard Test Method for Heat and Visible Smoke Release Rates for Materials and Products Using an Oxygen Consumption Calorimeter, ASTM International, West Conshohocken, PA, DOI: 10.1520/E1354-11B, [www.astm.org](http://www.astm.org)
- [10] Stoliarov, S.I., and Lyon, R.E., (2008) Thermo-Kinetic Model of Burning, Federal Aviation Administration Technical Note DOT/FAA/AR-TN08/17.

- [11] Siegel, R., and Howell, J., Thermal Radiation Heat Transfer, Taylor & Howell, New York, 2002.
- [12] Matsumoto, T., and Ono, A., (1995) Specific Heat Capacity and Emissivity Measurements of Ribbon-Shaped Graphite Using Pulse Current Heating, International Journal of Thermophysics 16: 267-275, <http://dx.doi.org/10.1007/BF01438977>
- [13] Li J., Stoliarov, S.I., (2013) Measurement of Kinetics and Thermodynamics of the Thermal Degradation for Non-charring Polymers, Combustion and Flame 160: 1153-1310, <http://dx.doi.org/10.1016/j.combustflame.2013.02.012>
- [14] Chase, M.W., Jr., (1998) NIST-JANAF Thermochemical Tables, 4<sup>th</sup> Edition, Journal of Physical and Chemical Reference Data 9:1-1951, <http://dx.doi.org/10.1063/1.555666>
- [15] Huggett, C., (1990) Estimation of Rate of Heat Release by Means of Oxygen Consumption Measurements, Fire and Materials 4: 61-65, <http://dx.doi.org/10.1002/fam.810040202>
- [16] Ohlemiller, T.J., Chapter 2-9, in The SFPE Handbook of Fire Protection Engineering, 3<sup>rd</sup> Edition, NFPA, Quincy, MA, 2002.